Area, perimeter and derivatives of a skin curve [☆]

Ho-Lun Cheng [a], Herbert Edelsbrunner [b,*]

[a] *Department of Computer Science, University of Illinois at Urbana-Champaign, Urbana, IL, USA*
[b] *Department of Computer Science, Duke University, Durham, and Raindrop Geomagic, Research Triangle Park, NC, USA*

Abstract

The body defined by a finite collection of disks is a subset of the plane bounded by a tangent continuous curve, which we call the skin. We give analytic formulas for the area, the perimeter, the area derivative, and the perimeter derivative of the body. Given the filtrations of the Delaunay triangulation and the Voronoi diagram of the disks, all formulas can be evaluated in time proportional to the number of disks.
© 2003 Elsevier B.V. All rights reserved.

Keywords: Computational geometry; Differential geometry; Skin curves; Voronoi diagrams; Delaunay triangulations; Filtrations; Disks; Hyperbolas; Area; Perimeter; Derivatives

1. Introduction

In this paper, we are concerned with a geometric design paradigm that uses weighted points to control planar geometric shapes with tangent continuous boundaries. Specifically, we give formulas for measuring the area, the perimeter, the area derivative, and the perimeter derivative of such shapes.

Motivation. The primary motivation for the work in this paper is the automated design of geometric shapes with variable connectivity. This is the central problem in topology optimization, which is a field

of research within mechanical engineering [1,2]. The shape is computed by iterative improvement within a global design cycle. The main ingredients to the methods are

- a data structure representing the geometric shape;
- a representation of the spatial domain that contains that shape;
- an objective function that drives the iterative improvement of the shape.

The main requirements for the shape data structure are flexibility and measurability. A single iteration of the design cycle determines local changes to the shape, and the data structure ought to be flexible enough to implement the changes in shape and its topology. The local changes are computed through a stability analysis of the shape, which is based on local and global measurements of size and size derivatives.

A viable data structure for geometric shape is the skin and body representation introduced in [10]. In three dimensions, a skin is a tangent continuous surface defined by a finite collections of spheres. Its ability to smoothly deform from one shape to another has been studied in [7], and an algorithm for constructing and maintaining a mesh representing the surface has been described in [5]. We are still lacking a fast algorithm that measures the skin surface and the subset of space it bounds. This paper describes such an algorithm for the two-dimensional case, where the skin is a tangent continuous curve defined by a finite collection of disks [8]. The problems in two and three dimensions are principally the same, except that there are more and mathematically more challenging cases in three dimensions. We thus believe that the results presented in this paper can be used as a blue-print for the development of similar measuring algorithms in three dimensions.

Results. Let $\mathcal{D}$ be a finite collection of disks in the plane. The geometric shape defined by $\mathcal{D}$ is a subset of the plane which we refer to as the *body* of $\mathcal{D}$. Its boundary is a closed and tangent continuous but not necessarily connected curve, which we refer to as the *skin* of $\mathcal{D}$. The area and the perimeter of the body are continuous functions $A, P : \mathbb{R}^{3n} \to \mathbb{R}$, where n is the number of disks. The domain has dimension $3n$ because each disk has three degrees of freedom, two for its center and one for its radius. In other words, each point, or *state* in $\mathbb{R}^{3n}$ uniquely defines a collection of n disks and thus a body and a skin. The derivatives of A and P at a state $\mathbf{z} \in \mathbb{R}^{3n}$ are linear functions $DA_{\mathbf{z}}, DP_{\mathbf{z}} : \mathbb{R}^{3n} \to \mathbb{R}$. Being linear, they can be written as scalar products, $DA_{\mathbf{z}}(\mathbf{t}) = \mathbf{a} \cdot \mathbf{t}$ and $DP_{\mathbf{z}}(\mathbf{t}) = \mathbf{p} \cdot \mathbf{t}$, where $\mathbf{t} \in \mathbb{R}^{3n}$ is the variable vector and $\mathbf{a}^{\mathrm{T}}, \mathbf{p}^{\mathrm{T}} \in \mathbb{R}^{3n}$ are the gradients of the two functions.

We give analytic formulas for computing the area, the perimeter, the area derivative, and the perimeter derivative of a body. These formulas are based on the alpha shape theory and the inclusion-exclusion formulas introduced in [9]. Given the filtrations of the Delaunay triangulation and the dual Voronoi diagram of the set of disks, these formulas can be evaluated in time $O(n)$.

Outline. Section 2 presents geometric background, including the filtrations of the Delaunay triangulation and the Voronoi diagram and the mixed complex, which decomposes the body and the skin into simple pieces. Section 3 explains how the two filtrations and the mixed complex can be used to derive analytic formulas for the area and the perimeter of a body. Section 4 gives the area and perimeter derivatives by specifying their gradients. Section 5 concludes the paper.

2. Geometric background

In this section, we introduce the Voronoi decomposition of a union of disks, the Delaunay decomposition of the union of orthogonal disks, and the mixed complex decomposition of an interpolation of the two unions.

Voronoi decomposition. Let $\mathcal{D}$ be a collection of disks $D_i = (z_i, r_i)$, for $0 \leqslant i \leqslant n - 1$. The radius r_i is either a non-negative real or a non-negative multiple of the imaginary unit, $i = \sqrt{-1}$. Equivalently, the square of the radius is a real number. We call D_i *imaginary* if $r_i^2 < 0$. Imaginary disks play an important role in our theory, in spite of the fact that they are ignored when we take the union, $F = \bigcup \mathcal{D}$, which is the portion of $\mathbb{R}^2$ covered by non-imaginary disks. The *power distance* of a point $x \in \mathbb{R}^2$ from D_i is $\pi_i(x) = \|x - z_i\|^2 - r_i^2$. The point x belongs to D_i iff $\pi_i(x) \leqslant 0$, and it belongs to F iff $\pi_j(x) \leqslant 0$ for at least one j. The *Voronoi polygon* of D_i is the set of points for which D_i minimizes the power distance,

$$\nu_i = \left\{ x \in \mathbb{R}^2 \mid \pi_i(x) \leqslant \pi_j(x), \forall j \right\}.$$

Assuming general position, each *Voronoi edge* is the intersection of two Voronoi polygons, $\nu_{ij} = \nu_i \cap \nu_j$, and each *Voronoi vertex* is the intersection of three, $\nu_{ijk} = \nu_i \cap \nu_j \cap \nu_k$. The *Voronoi diagram* is the collection of Voronoi polygons, edges and vertices. The Voronoi polygons cover all of $\mathbb{R}^2$ and they decompose the union of disks into convex regions of the form $\nu_i \cap F = \nu_i \cap D_i$, as illustrated in Fig. 1. The *dual complex* of this decomposition contains a simplex for each non-empty intersection of the convex regions. By assumption of general position we only have vertices $\sigma_i = z_i$, edges $\sigma_{ij} = z_i z_j$ and triangles $\sigma_{ijk} = z_i z_j z_k$. An example is shown in Fig. 1. We write $\sigma_i \leqslant \sigma_{ij} \leqslant \sigma_{ijk}$ to express that the simplices to the left are *faces* of the ones to their right. We may grow the disks continuously in a way such that the Voronoi diagram does not change. To do this, we use a parameter α with $\alpha^2 \in \mathbb{R}$, define $D_{i,\alpha}$ as the disk with center z_i and radius $(r_i^2 + \alpha^2)^{1/2}$, let $\mathcal{D}_\alpha$ be the collection of disks $D_{i,\alpha}$, and define $F_\alpha = \bigcup \mathcal{D}_\alpha$. The *$\alpha$-complex* K_α of $\mathcal{D}$ is the dual complex of $\mathcal{D}_\alpha$. For sufficiently large negative α^2, all disks are imaginary and the α-complex is empty. For sufficiently large positive α^2, every Voronoi polygon, edge and vertex has non-empty intersection with F_α, and the α-complex is the dual of the Voronoi diagram, which is referred to as the *Delaunay triangulation K* of $\mathcal{D}$. Similar to the radii, the parameter α takes on non-negative real values and non-negative real multiples of the imaginary unit. These values are totally ordered, and we have a nested sequence of alpha complexes,

$$\emptyset = K_{i\infty} \subseteq K_{\alpha_1} \subseteq K_{\alpha_2} \subseteq K_\infty = K,$$
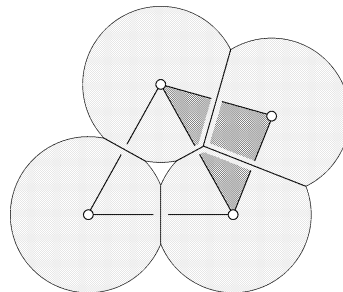

Fig. 1. The Voronoi decomposition of a union of four disks drawn on top of its dual complex, which consists of four vertices, six edges and one (dark shaded) triangle.

for $\alpha_1^2 \leqslant \alpha_2^2$. Since the Delaunay triangulation is a finite set, there are only finitely many different alpha complexes. We refer to the maximal nested sequence of pairwise different such complexes as the *alpha filtration* of the Delaunay triangulation.

Delaunay decomposition.   Using $\mathcal{D}$ and its Voronoi diagram, we construct a second collection $\mathcal{U}$ of disks $U_\iota = (y_\iota, s_\iota)$. Specifically, for each Voronoi vertex v_{ijk}, we have a disk with center $y_\iota = v_{ijk}$ and square radius $s_\iota^2 = \pi_i(y_\iota)$. By construction of y_ι, the square radius is also equal to $\pi_j(y_\iota)$ and to $\pi_k(y_\iota)$. With this choice of radius, we have $\|y_\iota - z_i\|^2 = s_\iota^2 + r_i^2$, which is the condition for U_ι and D_i to be *orthogonal*. Similarly, U_ι is orthogonal to D_j and to D_k. We refer to the collection $\mathcal{U}$ of thus constructed disks as the *orthogonal dual* of $\mathcal{D}$.

     The definition of orthogonal dual has a subtle but substantial flaw, which we remedy by compactifying the Voronoi diagram and the Delaunay triangulation. In doing so, we reveal a fundamental symmetry between the two. Specifically, we add a disk D_n with center z_n at infinity and radius $r_n = i\infty$ to $\mathcal{D}$. The effect of this addition can be visualized by drawing the Voronoi diagram and the Delaunay triangulation on the sphere. As illustrated in Fig. 2, the diagrams in $\mathbb{R}^2$ can be obtained by stereographic projection from z_n. We get a new Voronoi polygon whose vertices are all at infinity and can be interpreted as the endpoints of the formerly unbounded Voronoi edges. We also get z_n as a new Delaunay vertex, which is connected to the formerly extreme vertices of K via new Delaunay edges. Furthermore, each new Voronoi vertex v_{ijn} is the center of an infinitely large disk U_ι that is orthogonal to D_i and D_j. This is a half-plane whose bounding line passes through z_i and z_j.

     We now have complete symmetry between the two collection of disks. It is not difficult to see that the Voronoi polygon of the disk U_ι orthogonal to D_i, D_j and D_k is the Delaunay triangle σ_{ijk}. It follows that the Voronoi diagram of $\mathcal{U}$ is the Delaunay triangulation of $\mathcal{D}$, and symmetrically, the Delaunay triangulation of $\mathcal{U}$ is the Voronoi diagram of $\mathcal{D}$. The Delaunay triangulation K of $\mathcal{D}$ thus decomposes the union of orthogonal disks, $G = \bigcup \mathcal{U}$, into convex regions. We find that the dual complex of $\mathcal{U}$ is the collection of Voronoi vertices, edges and polygons that correspond to Delaunay simplices whose intersection with the union is non-empty. We have vertices v_{ijk}, edges v_{ij} and polygons v_i. We use a parameter β with $\beta^2 \in \mathbb{R}$ to grow the orthogonal disks to $U_{\iota,\beta} = (y_\iota, (s_\iota^2 + \beta^2)^{1/2})$. Let $\mathcal{U}_\beta$ be the collection of disks $U_{\iota,\beta}$, let $G_\beta = \bigcup \mathcal{U}_\beta$, and define the *$\beta$-complex* V_β of $\mathcal{U}$ as the dual complex of $\mathcal{U}_\beta$.
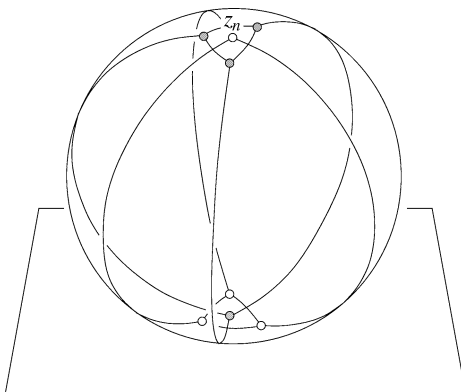

Fig. 2. Sketch of the compactified Voronoi diagram with shaded vertices and the dual Delaunay triangulation with white vertices.

For sufficiently large negative β^2, we get the empty complex, and for sufficiently large positive β^2, we get the Voronoi diagram V of $\mathcal{D}$. More generally, we have

$$\emptyset = V_{i\infty} \subseteq V_{\beta_1} \subseteq V_{\beta_2} \subseteq V_\infty = V,$$

for $\beta_1^2 \leqslant \beta_2^2$. The maximal subsequence of pairwise different such complexes is referred to as the *beta filtration* of the Voronoi diagram. Note that if we start with $\mathcal{D}_\alpha$ instead of $\mathcal{D}$ then we get orthogonal disks with the same centers but with different radii. Specifically, we get $\mathcal{U}_\beta$ with $\beta = i\alpha$ as the orthogonal dual. In other words, the two filtrations relate to each other via an anti-parallel correspondence in which K_α maps to $V_{i\alpha}$ and vice versa.

Skin and body. Given $\mathcal{D}$, the skin is a tangent continuous curve that differs from the boundary of F in two respects. First, it shrinks every disk by a factor $1/\sqrt{2}$, and second, it removes sharp corners by blending between adjacent disk boundaries. We use the vector space of quadratic functions to formally describe this curve. Recall that the circle bounding D_i is the zero-set of the corresponding power distance function, $\pi_i^{-1}(0)$. An affine combination of the π_i is a function

$$\pi(x) = \sum_{i=0}^{n} \gamma_i \pi_i(x) \quad \text{with } \sum_{i=0}^{n} \gamma_i = 1.$$

It is the power distance function of a new disk, which we denote

$$D = \sum_{i=0}^{n} \gamma_i D_i$$

and refer to as an *affine combination* of the D_i. The *affine hull* of $\mathcal{D}$, aff $\mathcal{D}$, is the set of all affine combinations. The affine combination D is a *convex combination* of the D_i if $\gamma_i \geqslant 0$ for all i, and the *convex hull* of $\mathcal{D}$, conv $\mathcal{D}$, is the set of all convex combinations. The final step in the construction shrinks all disks by a factor $1/\sqrt{2}$ while keeping their centers fixed. We use the superscript to denote shrinking and define $D_i^{1/2} = (z_i, r_i/\sqrt{2})$. The set of shrunken disks in the convex hulls is denoted as

$$(\text{conv}\,\mathcal{D})^{1/2} = \left\{ D^{1/2} \mid D \in \text{conv}\,\mathcal{D} \right\}.$$

The *body* of $\mathcal{D}$ is the union of shrunken convex combinations, and the *skin* is the boundary of that union,

$$\text{body}\,\mathcal{D} = \bigcup (\text{conv}\,\mathcal{D})^{1/2}, \qquad \text{skin}\,\mathcal{D} = \text{bd}\,\text{body}\,\mathcal{D}.$$

Fig. 3 illustrates these concepts. Recall that the orthogonal dual $\mathcal{U}$ of $\mathcal{D}$ is also a collection of disks. We refer to [10] for a proof that the skins of the two collections are the same and their bodies are complementary:

$$\text{body}\,\mathcal{D} \cap \text{body}\,\mathcal{U} = \text{skin}\,\mathcal{D} = \text{skin}\,\mathcal{U}, \tag{1}$$
$$\text{body}\,\mathcal{D} \cup \text{body}\,\mathcal{U} = \mathbb{R}^2. \tag{2}$$

Since $\mathcal{U}_{i\alpha}$ is the orthogonal dual of $\mathcal{D}_\alpha$, we also have skin $\mathcal{D}_\alpha = $ skin $\mathcal{U}_{i\alpha}$ for all $\alpha^2 \in \mathbb{R}$.

Mixed complex decomposition. If $\mathcal{D}$ contains only one disk D_i, then its skin is obviously a circle, namely the boundary S_i of $B_i = D_i^{1/2}$. Elementary algebraic calculations show that the envelope of the shrunken affine hull of two disks D_i and D_j is a hyperbola whose asymptotes form a right angle. We
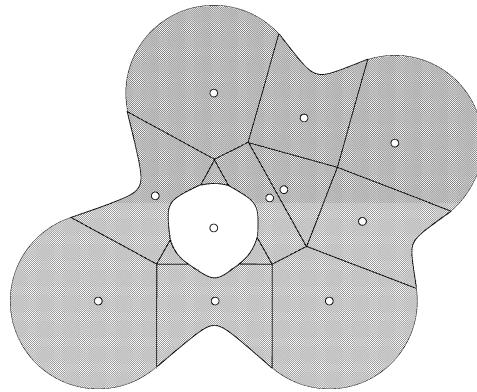
Fig. 3. The skin bounds the (shaded) body, which is the union of the shrunken convex combinations of the disks in Fig. 1. The portions of the mixed cells that decompose the body are shown together with the foci of their circles and hyperbolas.

denote the hyperbola by S_{ij} and the region bounded by the hyperbola by $B_{ij} = \bigcup (\mathrm{aff}\{D_i, D_j\})^{1/2}$. We use Property (1) to determine the skin of three disks D_i, D_j and D_k that form a hole, like the one in Fig. 1. The three disks define a single non-imaginary orthogonal disk U_ι, and the skin locally around the hole is the circle obtained by shrinking U_ι. We denote this circle by S_{ijk} and the closed complement of the disk it bounds by B_{ijk}. We will see shortly that the entire skin and body can be decomposed into instances of these three cases.

Let ν_* be a Voronoi polygon, edge or vertex and let σ_* be the dual Delaunay vertex, edge or triangle. Their dimensions are supplementary, $\dim \nu_* + \dim \sigma_* = 2$. The corresponding *mixed cell* is the Minkowski sum of scaled copies, $\mu_* = \frac{1}{2}\nu_* + \frac{1}{2}\sigma_*$, which is a convex polygon. The *mixed complex* M of $\mathcal{D}$ consists of all mixed cells together with their edges and vertices. Any two mixed cells are either disjoint or intersect in a common edge or vertex, and together they cover $\mathbb{R}^2$. As explained in [8,10], the mixed cells decompose the skin into circle and hyperbola pieces. We have three types of mixed cells, distinguished by the number of indices, which is one more than the dimension of the corresponding Delaunay simplex, $p = \dim \sigma_*$. Instances of all three cases can be seen in Fig. 3.

Case $p = 0$. The mixed cell $\mu_i = \frac{1}{2}(\nu_i + \sigma_i)$ is the translate of a scaled Voronoi polygon. Within the window provided by μ_i, the skin is a circle.

Case $p = 1$. The mixed cell $\mu_{ij} = \frac{1}{2}(\nu_{ij} + \sigma_{ij})$ is the scaled Minkowski sum of a Voronoi edge and its dual Delaunay edge, which is a rectangle. Within the rectangular window, the skin is a hyperbola.

Case $p = 2$. The mixed cell $\mu_{ijk} = \frac{1}{2}(\nu_{ijk} + \sigma_{ijk})$ is the translate of a scaled Delaunay triangle. Within the window provided by μ_{ijk}, the skin is a circle.

In general, the skin within a mixed cell is $\mu_* \cap \mathrm{skin}\,\mathcal{D} = \mu_* \cap S_*$, and the body is $\mu_* \cap \mathrm{body}\,\mathcal{D} = \mu_* \cap B_*$. Recall that B_* is the union of a family obtained by shrinking the disks in the affine hull of one, two or three disks. The smallest disk in this family is significant in describing S_* and B_*. We call the center and the square radius of that disk the *focus* z_* and the *age* g_* of S_* and B_*. In case $p = 0$, the focus is the center of D_i and the age is $g_i = r_i^2/2$. In case $p = 1$, the focus is the apex z_{ij} of the hyperbola, and a formula for the age will be given in Section 4. In case $p = 2$, the focus is $z_{ijk} = y_\iota$ and the age is $g_{ijk} = -s_\iota^2/2$.

3. Size

In this section, we study relations between the skin and the alpha and beta filtrations, and we use these relations to derive formulas for measuring the sizes of the skin, the body, and their decompositions by the mixed complex.

Results. We begin by stating the results. We consider four measures and express each by a sum over all mixed cells. For each μ_*, we consider the area of the body within μ_*, the length of the skin within μ_*, the length of its boundary within the body, and the number of intersections of its boundary with the skin:

$$A_* = \text{area}(\mu_* \cap B_*), \qquad P_* = \text{length}(\mu_* \cap S_*),$$

$$L_* = \text{length}(\text{bd}\,\mu_* \cap B_*), \qquad N_* = \text{card}(\text{bd}\,\mu_* \cap S_*).$$

The area and perimeter are important measures in their own right, and the length and cardinality of the decompositions are used in the formulas of the area and perimeter derivatives given in Section 4.

Size Theorem. *The area and perimeter of the body of a finite collection of disks, the total length of the decomposition of the body, and the total number of points in the decomposition of the skin are*

$$A = \sum_i A_i + \sum_{ij} A_{ij} + \sum_{ijk} A_{ijk}, \qquad P = \sum_i P_i + \sum_{ij} P_{ij} + \sum_{ijk} P_{ijk},$$

$$L = \sum_{ij} L_{ij}, \qquad N = \sum_{ij} N_{ij}.$$

The sums for A and P range over all vertices σ_i, over all edges σ_{ij}, and over all triangles σ_{ijk} of the Delaunay triangulation. Each line segment and each point in the decompositions of the body and the skin belong to exactly two mixed cells. Exactly one of any such pair is a double-index mixed cell, which explains why the sums for L and N range only over this one type. In the remainder of this section, we express all terms in the sums by formulas involving the the centers and radii of the given and the orthogonal disks. Formulas for the A_* are given in Eqs. (3), (5) and (9), formulas for the P_* are given in Eqs. (4), (6) and (10), and formulas for the L_{ij} and N_{ij} are given in Eqs. (7) and (8).

Disks. A single-index mixed cell μ_i is obtained by shrinking the Voronoi polygon ν_i by a factor $1/2$ towards the center z_i of the corresponding disk D_i. Its intersection with the body is $\mu_i \cap B_i$, and we recall that B_i is obtained by shrinking D_i by a factor $1/\sqrt{2}$ towards the same point z_i. We get the same by first growing D_i to $D_{i,r_i} = (z_i, \sqrt{2}r_i)$, then intersecting ν_i with D_{i,r_i}, and finally shrinking the intersection by a factor $1/2$. This is illustrated in Fig. 4. Recall that A_i and P_i are the area of the body and the length of the skin, both clipped to within μ_i. There is more than one way to compute the two, and we choose to use inclusion-exclusion, as described in [9]. To explain this, we introduce the *star* of z_i in K_{r_i}, which contains all simplices that contain z_i, and the *link*, which contains all faces of simplices in the star that do not contain z_i,

$$\text{St}_{r_i} z_i = \{\tau \in K_{r_i} \mid z_i \leqslant \tau\}, \qquad \text{Lk}_{r_i} z_i = \{\sigma \in K_{r_i} \mid z_i \not\leqslant \sigma \leqslant \tau \in \text{St}_{r_i} z_i\}.$$
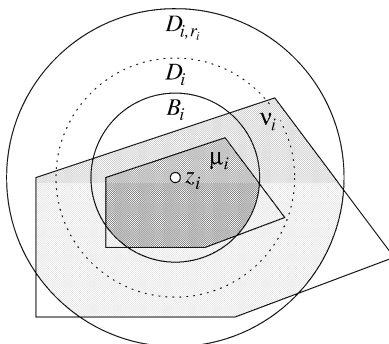
Fig. 4. The light shaded intersection of the Voronoi polygon with the grown disk is similar to the dark shaded intersection of the mixed cell with the shrunken disk.

We note that the (-1)-dimensional simplex, $\emptyset$, is necessarily an element of the link. For each simplex $\sigma \in \text{Lk}_{r_i} z_i$, consider the piece of the circle $C_{i,r_i} = \text{bd}\, D_{i,r_i}$ in the influence regions of the disks D_{j,r_i} that span σ,

$$C_{i,r_i}^{\sigma} = \{x \in C_{i,r_i} \mid \pi_j(x) \leqslant \pi_i(x), \forall z_j \leqslant \sigma\}.$$

For example, $C_{i,r_i}^{\emptyset} = C_{i,r_i}$, and $C_{i,r_i}^{\{z_j\}}$ is the arc on the other side of the line separating ν_i and ν_j. Similarly, let D_{i,r_i}^{σ} be the piece of the disk D_{i,r_i} in the influence regions of the D_{j,r_i}, with $z_j \leqslant \sigma$. Analytic formulas for the length and area of these pieces are not difficult to compute. The portions inside ν_i can be written as alternating sums of these pieces, and we get the area and the perimeter inside μ_i after appropriate scaling:

$$A_i = \frac{1}{4} \sum_{\sigma} (-1)^{\dim \sigma + 1} \, \text{area}\big(D_{i,r_i}^{\sigma}\big), \tag{3}$$

$$P_i = \frac{1}{2} \sum_{\sigma} (-1)^{\dim \sigma + 1} \, \text{length}\big(C_{i,r_i}^{\sigma}\big). \tag{4}$$

Both sums range over all simplices σ in the link of z_i in K_{r_i}. We get the first terms in the expression for A and P in the Size Theorem by summing the A_i and P_i over all single-index mixed cells μ_i.

Hyperbolas. A double-index mixed cell μ_{ij} is obtained by shrinking the Minkowski sum of the two corresponding Voronoi and Delaunay edges by a factor $1/2$ towards the focus z_{ij} of the corresponding hyperbola. This focus is also the intersection point of the lines spanned by the edges, $z_{ij} = \text{aff}\, \sigma_{ij} \cap \text{aff}\, \nu_{ij}$. The points on the line of the Delaunay edge are centers of disks in the shrunken affine hull of D_i and D_j. We translate and rotate the configuration such that σ_{ij} lies on the (horizontal) x_1-axis and ν_{ij} lies on the (vertical) x_2-axis of our Cartesian system, as drawn in Fig. 5. In this normalized form, z_{ij} lies at the origin and the equation of the hyperbola S_{ij} is $-x_1^2 + x_2^2 = g_{ij}$. We compute the length and the area it bounds inside μ_{ij} by integration. Assuming $z_{ij} \in \mu_{ij}$, we consider the upper right quadrant, which is a rectangle $[0, w] \times [0, h]$, with $w = \|z_{ij} - z_j\|/2$ and $h = \|z_{ij} - z_{ijl}\|/2$. Assuming $g_{ij} \geqslant 0$, we get $x_2 = (x_1^2 + g_{ij})^{1/2}$ as a real valued function over the entire interval $0 \leqslant x_1 \leqslant w$. Assuming $h^2 \geqslant w^2 + g_{ij}$, the area of B_{ij} inside the upper right quadrant is
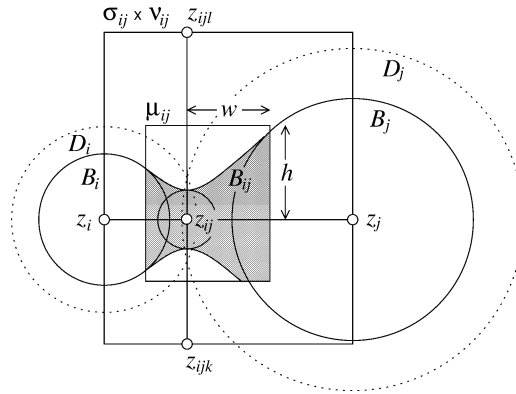
Fig. 5. The hyperbola within the mixed cell is the envelope of the shrunken disks in the affine hull of D_i and D_j.

$$A_{ij}^{\mathrm{ur}} = \int_{x_1=0}^{w} \sqrt{x_1^2 + g_{ij}}\, \mathrm{d}x_1 = \frac{1}{2}\Big[x_1\sqrt{x_1^2 + g_{ij}} + g_{ij}\ln\Big(x_1 + \sqrt{x_1^2 + g_{ij}}\Big)\Big]_0^w$$

$$= \frac{1}{2}\bigg(wH + g_{ij}\ln\frac{w+H}{\sqrt{g_{ij}}}\bigg), \tag{5}$$

where $H = (w^2 + g_{ij})^{1/2}$ is the value of x_2 for $x_1 = w$. The length of the hyperbola within the upper right quadrant of μ_{ij} is

$$P_{ij}^{\mathrm{ur}} = \int_{x_1=0}^{w} \sqrt{1 + \bigg(\frac{\mathrm{d}x_2}{\mathrm{d}x_1}\bigg)^2}\, \mathrm{d}x_1 = \int_{x_1=0}^{w} \sqrt{\frac{2x_1^2 + g_{ij}}{x_1^2 + g_{ij}}}\, \mathrm{d}x_1 = \sqrt{g_{ij}} \int_{t=0}^{w/\sqrt{g_{ij}}} \sqrt{\frac{2t^2 + 1}{t^2 + 1}}\, \mathrm{d}t, \tag{6}$$

where we define $t = x_1/\sqrt{g_{ij}}$ to get the last line. The result is an example of an elliptic integral, which is analytically not soluble [3], but for which fast numerical routines have been developed and are available as part of public numerical software packages.

In the configuration drawn in Fig. 5, the total area A_{ij} and perimeter P_{ij} can be obtained by adding the portions in the four quadrants. Within each quadrant, the computations are symmetric, except for a small modification necessary in the lower right quadrant, in which the hyperbola does not reach the right side of the rectangle. We now give an analysis of all generic cases and show that A_{ij} and P_{ij} are generally sums of four terms each, although some of the terms can be negative. We distinguish configurations by considering the age of the hyperbola and the signed distances of the focus from the four sides. For positive age, B_{ij} is connected and sandwiched between the upper and lower branches of the hyperbola, as in Fig. 5, while for negative age, B_{ij} consists of two regions separated by the left and right branches of the hyperbola. After a rigid motion that moves the focus to the origin and the Delaunay edge onto the horizontal coordinate axis, the mixed cell is a rectangle $[-w_{ij}, w_{ji}] \times [-h_{ij}, h_{ji}]$. The lines spanned by the four sides decompose the plane into nine regions, and we distinguish configurations depending on which of these regions contains the origin. In each case, we compute the area and perimeter by summing the portions inside four axis-aligned rectangular boxes, each one defined by the origin and one of the four corners of μ_{ij}. To get the correct result, we take the measurements inside a box positive or negative depending on whether the two corresponding w- and h-values have the same or different signs. When

we compute the area and perimeter inside a box, we distinguish between the case in which the defining corner belongs to the body, and the complementary case in which it does not. Finally, we get the A_{ij} and P_{ij} by summing the results for the four quadrants. We get the second terms in the expressions for A and P in the Size Theorem by summing the A_{ij} and P_{ij} over all double-index mixed cells μ_{ij}.

Boundary of mixed cells. The computations of L_{ij} and N_{ij} are similar. Consider the intersection of the four sides of μ_{ij} with the body, or equivalently with B_{ij}, as illustrated in Fig. 6. Each side intersects B_{ij} in a line segment or the complement of a line segment, and we use W_{ij}, W_{ji}, H_{ij} and H_{ji} to denote their lengths. Each intersection has zero, one or two endpoints in the interior of the corresponding side of μ_{ij}, and we let E_{ij}, E_{ji}, F_{ij} and F_{ji} be these numbers. With this notation, we have

$$L_{ij} = W_{ij} + W_{ji} + H_{ij} + H_{ji}, \tag{7}$$
$$N_{ij} = E_{ij} + E_{ji} + F_{ij} + F_{ji}. \tag{8}$$

We compute L_{ij} and N_{ij} using the filtrations of the Delaunay triangulation and the Voronoi diagram. By the reasoning illustrated in Fig. 4, H_{ij} is half the length of the intersection between the Voronoi edge v_{ij} and the disk D_{i,r_i}. The length of this intersection can be computed by inclusion-exclusion based on whether or not σ_{ij} and the two triangles σ_{ijk} and σ_{ijl} that share it belong to K_{r_i}. Recall that F_{ij} is the number of endpoints of that intersection in the interior of v_{ij}. This is also 2 minus the number of triangles that share σ_{ij} and belong to K_{r_i}. Similarly, we get H_{ji} and F_{ji} by switching i and j. Furthermore, we get W_{ij}, W_{ji}, E_{ij} and E_{ji} the same way from the beta filtration, keeping in mind that it presents the complement, so we perform complementary measurements. Finally, we get L and N in the Size Theorem by summing the L_{ij} and N_{ij} over all double-index mixed cells μ_{ij}.

Disk complements. A triple-index mixed cell μ_{ijk} is obtained by shrinking the Delaunay triangle σ_{ijk} by a factor $1/2$ towards the center $z_{ijk} = y_\iota$ of the corresponding orthogonal disk U_ι. Its intersection with the body is $\mu_{ijk} = B_{ijk}$, and we recall that B_{ijk} is obtained by shrinking U_ι by a factor $1/\sqrt{2}$ towards the same point z_{ijk} and taking the complement. Similar to the single-index case, we get the same by first
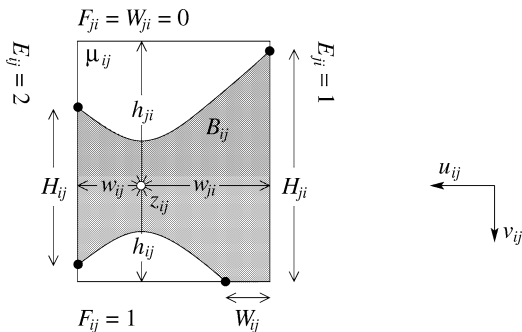

Fig. 6. Notation for the length of rectangle sides clipped within the body and for the distances of the focus from the four sides.
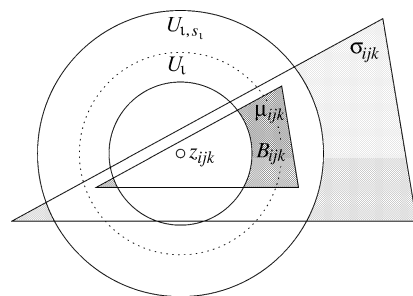
Fig. 7. The light shaded intersection of the Delaunay triangle with the complement of the grown orthogonal disk is similar to the dark shaded intersection of the mixed cell with the complement of the shrunken orthogonal disk.

growing U_ι to $U_{\iota,s_\iota} = (y_\iota, \sqrt{2}s_\iota)$, then intersecting σ_{ijk} with U_{ι,s_ι}, and finally shrinking the intersection by a factor $1/2$. This is illustrated in Fig. 7. We use again inclusion-exclusion to compute the length P_{ijk} of the skin and the area A_{ijk} of the body within μ_{ijk}. Consider the star and the link of $y_\iota = v_{ijk}$,

$$\mathrm{St}_{s_\iota} \, y_\iota = \{v \in V_{s_\iota} \mid y_\iota \leqslant v\}, \qquad \mathrm{Lk}_{s_\iota} \, y_\iota = \{v \in V_{s_\iota} \mid y_\iota \not\leqslant v \leqslant v \in \mathrm{St}_{s_\iota} \, y_\iota\}.$$

Note again that the empty Voronoi polygon, $\emptyset$, is necessarily an element of the link. For each Voronoi vertex, edge and polygon $v \in \mathrm{Lk}_{s_\iota} \, y_\iota$, let C^v_{ι,s_ι} be the piece of the circle $C_{\iota,s_\iota} = \mathrm{bd}\, U_{\iota,s_\iota}$ in the influence regions of the disks U_{κ,s_ι} whose centers span v. Similarly, let U^v_{ι,s_ι} be the piece of the disk U_{ι,s_ι} in the influence regions of the disks U_{κ,s_ι} with $y_\kappa \leqslant v$. The portions inside σ_{ijk} can be written as alternating sums of these pieces, and we get the area and the perimeter inside μ_{ijk} after scaling and taking the complement:

$$A_{ijk} = \mathrm{area}(\mu_{ijk}) - \frac{1}{4} \sum_v (-1)^{\dim v + 1} \mathrm{area}\big(U^v_{\iota,s_\iota}\big), \tag{9}$$

$$P_{ijk} = \frac{1}{2} \sum_v (-1)^{\dim v + 1} \mathrm{length}\big(C^v_{\iota,s_\iota}\big). \tag{10}$$

Both sums range over all Voronoi vertices and edges v in the link of y_ι in V_{s_ι}. We note that these sums can be simplified by replacing paths in the link by single edges. Specifically, each Voronoi polygon v_i in the star contributes an open path of edges and vertices to the link of y_ι, and this path may be replaced by a single edge connecting the two ends. This replacement is akin to triangulating v_i in such a way that none of the diagonals ends at y_ι. The replacement does not change the result of the sum because all vertices on the path define bisectors that pass through the corner z_i of the Delaunay triangle. Finally, we get the third terms in the expressions for A and P in the Size Theorem by summing the A_{ijk} and P_{ijk} over all triple-index mixed cells μ_{ijk}.

4. Derivatives

In this section, we give a complete description of the area and perimeter derivatives of a body.

Results. We begin by stating the results. Since the complete statements are unwieldy, we present a generic formulation of the derivatives that can be developed using substitutions given subsequently in this section.

Derivative Theorem. *Let X be the area or perimeter function of the body defined by a collection of n disks with state $\mathbf{z} \in \mathbb{R}^{3n}$. Its derivative is $\mathrm{D}X_{\mathbf{z}}(\mathbf{t}) = \mathbf{x} \cdot \mathbf{t}$, where*

$$\begin{bmatrix} \mathbf{x}_{3i+1} \\ \mathbf{x}_{3i+2} \end{bmatrix}^{\mathrm{T}} = \frac{\mathrm{d}X_i}{\mathrm{d}z_i} + \sum_j \frac{\mathrm{d}X_{ij}}{\mathrm{d}z_i} + \sum_{j,k} \frac{\mathrm{d}X_{ijk}}{\mathrm{d}z_i}, \qquad \mathbf{x}_{3i+3} = \frac{\mathrm{d}X_i}{\mathrm{d}r_i^2} + \sum_j \frac{\mathrm{d}X_{ij}}{\mathrm{d}r_i^2} + \sum_{j,k} \frac{\mathrm{d}X_{ijk}}{\mathrm{d}r_i^2},$$

for all $0 \leqslant i < n$.

We write $\mathbf{a}$ for $\mathbf{x}$ if $X = A$ is the area function, and $\mathbf{p}$ for $\mathbf{x}$ if $X = P$ is the perimeter function. In both cases, the sums in the theorem range over all vertices σ_j and all edges σ_{jk} in the link of σ_i in the Delaunay triangulation of $\mathcal{D}$. Some of the terms might be zero, and an efficient way to determine the
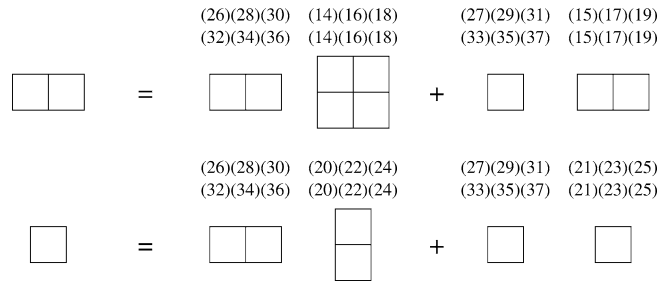
Fig. 8. The matrices are labeled by the equations that can be substituted to give the derivatives of the area and the perimeter with respect to z_i in the first and with respect to r_i^2 in the second row.

non-zero ones uses the alpha and beta filtrations, as described in Section 2. For each single, double and triple index $*$, we get the derivatives by separating the contributions of sliding and aging,

$$\frac{dX_*}{dz_i} = \frac{dX_*}{dz_*}\frac{dz_*}{dz_i} + \frac{dX_*}{dg_*}\frac{dg_*}{dz_i}, \qquad \frac{dX_*}{dr_i^2} = \frac{dX_*}{dz_*}\frac{dz_*}{dr_i^2} + \frac{dX_*}{dg_*}\frac{dg_*}{dr_i^2}.$$

The derivatives with respect to z_i are given in Eqs. (14)–(19), and the ones with respect to r_i^2 are given in Eqs. (20)–(25). The derivatives of A_* are given in Eqs. (26)–(31), and the derivatives of P_* are given in Eqs. (32)–(37). As illustrated in Fig. 8, the terms in the above equations are matrices. In computing the formulas, we exploit the linearity of the derivative and consider each disk separately. We also distinguish between the motion of a disk, which is caused by varying its center, and its growth, which is caused by increasing or decreasing its radius. As can be seen from the statement of the Derivative Theorem, we look at each mixed cell separately, and we determine how motion and growth affect the mixed cells and the skin and body within the cells. The change of the skin and body is the accumulation of the changes that happen within individual mixed cells. We begin with a detailed look at how a hyperbola depends on the two disks that define it.

Focus and age of a hyperbola. We express the focus and age of a hyperbola in terms of the centers and radii of the two defining disks, D_i and D_j. See Fig. 9 for the notation used for the computations. We let $2r_{ij}$ be the distance between the intersection points of the two circles, which is imaginary if the disks are disjoint. The square distances of the centers to the bisector are $4w_{ij}^2 = r_i^2 - r_{ij}^2$ and $4w_{ji}^2 = r_j^2 - r_{ij}^2$. We take w_{ij} and w_{ji} as positive or negative such that $\zeta_{ij} = 2w_{ij} + 2w_{ji}$ is the Euclidean distance between z_i and z_j. We have $r_i^2 - r_j^2 = 4w_{ij}^2 - 4w_{ji}^2 = \zeta_{ij}(2w_{ij} - 2w_{ji})$. From this, we get equations for the distance between z_i and the bisector, for the focus of the hyperbola, which is z_i plus $2w_{ij}$ times the unit vector from z_i to z_j, and for the age, which is $r_{ij}^2/2$:

$$2w_{ij} = \frac{1}{2}\left(\zeta_{ij} + \frac{r_i^2 - r_j^2}{\zeta_{ij}}\right), \tag{11}$$

$$z_{ij} = \frac{1}{2}\left((z_i + z_j) - \frac{r_i^2 - r_j^2}{\zeta_{ij}^2}(z_i - z_j)\right), \tag{12}$$

$$g_{ij} = \frac{1}{8}\left(2(r_i^2 + r_j^2) - \zeta_{ij}^2 - \frac{(r_i^2 - r_j^2)^2}{\zeta_{ij}^2}\right). \tag{13}$$
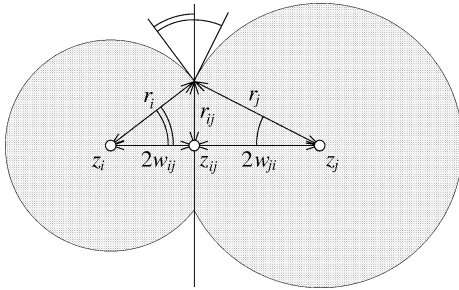
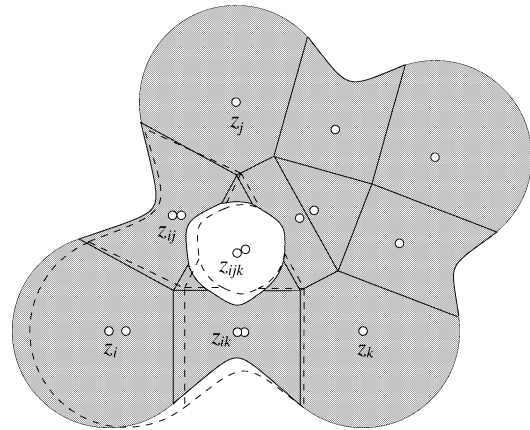Fig. 9. Two disks define various lengths and angles.

Fig. 10. The solid lines bound and decompose the initial body. The dashed lines indicate how the body and its decomposition change as a reaction to the motion of D_i.

Let $\varphi_{ij} = \arccos \frac{2w_{ij}}{r_i}$ be the angle at z_i, as shown in Fig. 9. This is also the angle between the bisector and the tangent at the point where the bisector intersects the circle. It follows that $\varphi_{ij} + \varphi_{ji}$ is the angle between the two circles at each intersection point.

Propagation of motion. As illustrated in Fig. 10, the motion of a disk D_i affects the body within all mixed cells whose indices include i. No other foci and ages change, although the boundary between the first and second layers of mixed cells around μ_i slide. We may ignore the sliding of any edge in the mixed complex because, to a first order of approximation, the gain and loss on its two sides cancel each other. However, we cannot neglect the sliding and aging of the circles and hyperbolas within the mixed cells. We consider the three types of mixed cells in turn.

Case $p = 0$. The circle within μ_i slides the same way the disk D_i moves, and the age of the circle remains constant. Hence

$$\frac{dz_i}{dz_i} = \begin{bmatrix} 1 & 0 \\ 0 & 1 \end{bmatrix}, \tag{14}$$

$$\frac{dg_i}{dz_i} = [\, 0 \quad 0 \,]. \tag{15}$$

Case $p = 1$. The hyperbola within μ_{ij} both slides and ages. We compute the rates of these changes in the orthonormal coordinate frame spanned by $u_{ij} = (z_i - z_j)/\|z_i - z_j\|$ and $v_{ij} = (z_{ijk} - z_{ijl})/\|z_{ijk} - z_{ijl}\|$, which is shown in Fig. 6. Assuming z_j is the origin, we have $z_i = (\zeta_{ij}, 0)$ and $z_{ij} = (2w_{ji}, 0)$ in this frame. The derivative of the focus with respect to the moving center is

$$\frac{dz_{ij}}{dz_i} = \left[\frac{dz_{ji}}{d\zeta_{ij}}, \frac{dz_{ji}}{d\eta_{ij}} \right] \cdot \begin{bmatrix} u_{ij}^T \\ v_{ij}^T \end{bmatrix}, \tag{16}$$

where

$$\frac{dz_{ij}}{d\zeta_{ij}} = \frac{d2w_{ji}}{d\zeta_{ij}} \cdot u_{ij} = \left(\frac{1}{2} + \frac{r_i^2 - r_j^2}{\zeta_{ij}^2} \right) \cdot u_{ij}, \qquad \frac{dz_{ij}}{d\eta_{ij}} = \frac{2w_{ji}}{\zeta_{ij}} \cdot v_{ij} = \left(\frac{1}{2} - \frac{r_i^2 - r_j^2}{\zeta_{ij}^2} \right) \cdot v_{ij}$$

are obtained from Eq. (11), after switching i and j. The matrix on the right in Eq. (16) transforms the input vector into the coordinate frame spanned by u_{ij} and v_{ij}. The age of the hyperbola is insensitive to sliding in the v_{ij}-direction, so we get the derivative of the age by differentiating Eq. (13) with respect to ζ_{ij}:

$$\frac{\mathrm{d}g_{ij}}{\mathrm{d}z_i} = \frac{1}{4}\left(-\zeta_{ij} + \frac{(r_i^2 - r_j^2)^2}{\zeta_{ij}^3}\right) \cdot u_{ij}^{\mathrm{T}}. \tag{17}$$

Case $p = 2$. The circle within μ_{ijk} both slides and ages. The sliding is restricted to the bisector defined by D_j and D_k. We may compute the new focus z_{ijk} by projecting the new focus z_{ij} onto that bisector, with the direction of the projection being orthogonal to the new edge σ_{ij}. We again separate the motion of z_i along u_{ij} from that along v_{ij} and write η_{ij} for the coordinate of z_i along the v_{ij}-direction. We get

$$\frac{\mathrm{d}z_{ijk}}{\mathrm{d}z_i} = \left[\frac{\mathrm{d}z_{ijk}}{\mathrm{d}\zeta_{ij}}, \frac{\mathrm{d}z_{ijk}}{\mathrm{d}\eta_{ij}}\right] \cdot \begin{bmatrix} u_{ij}^{\mathrm{T}} \\ v_{ij}^{\mathrm{T}} \end{bmatrix}, \tag{18}$$

where

$$\frac{\mathrm{d}z_{ijk}}{\mathrm{d}\zeta_{ij}} = \frac{\mathrm{d}2w_{ji}}{\mathrm{d}\zeta_{ij}} \cdot u_{ij} + \tan\psi_{ijk}\frac{\mathrm{d}2w_{ji}}{\mathrm{d}\zeta_{ij}} \cdot v_{ij} = \left(\frac{1}{2} + \frac{r_i^2 - r_j^2}{\zeta_{ij}^2}\right)(u_{ij} + \tan\psi_{ijk} \cdot v_{ij}),$$

$$\frac{\mathrm{d}z_{ijk}}{\mathrm{d}\eta_{ij}} = -\frac{2h_{ij}}{\zeta_{ij}}\,(u_{ij} + \tan\psi_{ijk} \cdot v_{ij}),$$

ψ_{ijk} is the angle from σ_{ij} to the bisector defined by D_j and D_k, and $2h_{ij}$ is the distance between z_{ij} and z_{ijk}. The relation for the derivative with respect to η_{ij} is illustrated in Fig. 11. We may use Eq. (11) to express $2h_{ij}$ in terms of radii and distances defined by orthogonal disks. The first matrix on the right side of Eq. (18) has rank one because z_{ijk} slides along a fixed line that is independent of the motion of z_i. To compute the rate of aging, we consider the disk $U_\iota = (y_\iota, s_\iota)$ orthogonal to D_i, D_j and D_k. We have $\|y_\iota - z_j\|^2 = 4w_{jk}^2 + 4h_{jk}^2$, since $2w_{jk} = \|z_j - z_{jk}\|$ and $2h_{jk} = \|z_{jk} - y_\iota\|$ are the distance
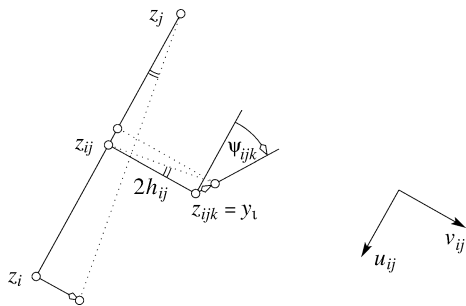

Fig. 11. The motion of z_i normal to the edge $\sigma_{ij} = z_i z_j$ causes the focus z_{ijk} to slide along the bisector defined by D_j and D_k.
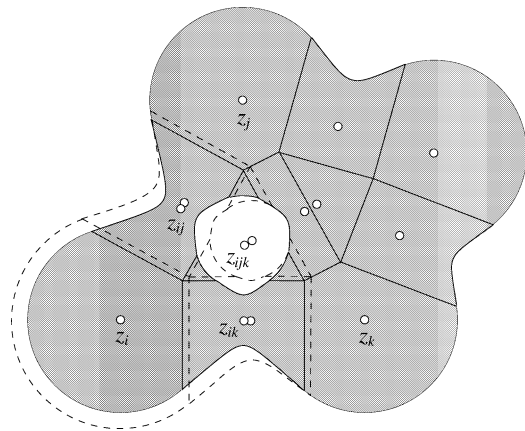
Fig. 12. The solid lines bound and decompose the initial body. The dashed lines indicate how the body and its decomposition change as a reaction to the growth of D_i.

components normal and parallel to the bisector defined by D_j and D_k, which contains $y_\iota = z_{ijk}$. This implies $s_\iota^2 = -r_j^2 + 4w_{jk}^2 + 4h_{jk}^2$. Since the derivative of the age is minus one half that of s_ι^2, and since r_j and w_{jk} remain constant, we have

$$\frac{\mathrm{d}g_{ijk}}{\mathrm{d}z_i} = -2h_{jk}\frac{\mathrm{d}2h_{jk}}{\mathrm{d}z_i}. \tag{19}$$

The motion of D_i pushes y_ι along the bisector, which implies that the rate at which $2h_{jk}$ changes is equal to the rate at which y_ι slides. As illustrated in Fig. 11, that rate is $1/\cos\psi_{ijk}$ times the rate at which the projection of y_ι slides along σ_{ij}. Using Eq. (18), we get

$$\frac{\mathrm{d}2h_{jk}}{\mathrm{d}z_i} = \frac{1}{\cos\psi_{ijk}}\left[\frac{\mathrm{d}2w_{ji}}{\mathrm{d}\zeta_{ij}}, -\frac{2h_{ij}}{\zeta_{ij}}\right]\cdot\begin{bmatrix}u_{ij}^{\mathrm{T}} \\ v_{ij}^{\mathrm{T}}\end{bmatrix}.$$

Propagation of growth. We grow a disk D_i by varying its square radius. Similar to motion, all mixed cells whose indices include i change and contribute to the derivative. This is illustrated in Fig. 12. Again, we consider the three types of mixed cells in turn.

Case $p = 0$. The circle within μ_i does not slide but it ages at the rate half the growth rate. Hence

$$\frac{\mathrm{d}z_i}{\mathrm{d}r_i^2} = \begin{bmatrix}0 \\ 0\end{bmatrix}, \tag{20}$$

$$\frac{\mathrm{d}g_i}{\mathrm{d}r_i^2} = 1/2. \tag{21}$$

Case $p = 1$. The hyperbola within μ_{ij} both slides and ages. The first rate is obtained by differentiating Eq. (12), and the second by differentiating Eq. (13):

$$\frac{\mathrm{d}z_{ij}}{\mathrm{d}r_i^2} = -\frac{1}{2\zeta_{ij}}\cdot u_{ij}, \tag{22}$$

$$\frac{\mathrm{d}g_{ij}}{\mathrm{d}r_i^2} = \frac{1}{4}\left(1 - \frac{r_i^2 - r_j^2}{\zeta_{ij}^2}\right). \tag{23}$$

Case $p = 2$. The circle within μ_{ijk} both slides and ages. As before, we use the fact that z_{ijk} is the projection of z_{ij} onto the bisector defined by D_j and D_k in a direction orthogonal to σ_{ij}. Using Eq. (22), we get

$$\frac{\mathrm{d}z_{ijk}}{\mathrm{d}r_i^2} = -\frac{1}{2\zeta_{ij}}\cdot u_{ij} - \frac{\tan\psi_{ijk}}{2\zeta_{ij}}\cdot v_{ij}. \tag{24}$$

We compute the rate of aging by considering the disk $U_\iota = (y_\iota, s_\iota)$ orthogonal to D_i, D_j and D_k, as before. We again have $s_\iota^2 = -r_j^2 + 4w_{jk}^2 + 4h_{jk}^2$. The growth of D_i pushes y_ι along the bisector, and the derivative of $2h_{jk}$ with respect to r_i^2 is the length of the derivative of z_{ijk} with respect to r_i^2, which is given in (24). Finally, we use that the derivative of the age is minus one half that of s_ι^2. Since r_j and w_{jk} remain constant, the derivative of the age is therefore minus $2h_{jk}$ times $\mathrm{d}2h_{jk}/\mathrm{d}r_i^2$, which is

$$\frac{\mathrm{d}g_{ijk}}{\mathrm{d}r_i^2} = -2h_{jk}\frac{1 + \tan^2\psi_{ijk}}{4\zeta_{ij}^2}. \tag{25}$$

Elementary derivatives for area.　　As before, we consider the three types of mixed cells in turn.

Case $p = 0$. Within a mixed cell μ_i, the body is a disk and the skin is a circle. The boundary of $\mu_i \cap B_i$ consists of circular arcs and straight line segments. Using the notation of Section 3, the length of that boundary is $P_i + \sum_j H_{ij}$, where P_i is the total length of the arcs, and H_{ij} is the length of the shrunken Voronoi edge v_{ij} clipped to within B_i. When we slide the center along a vector t_i, then the area of B_i within μ_i changes at a rate that depends on the lengths of the line segments and the angles they form with t_i. Specifically, that rate is $(\mathrm{d}A_i/\mathrm{d}z_i) \cdot t_i$, with

$$\frac{\mathrm{d}A_i}{\mathrm{d}z_i} = \sum_j \left(H_{ij} \cdot u_{ij}^{\mathrm{T}}\right). \tag{26}$$

Note that the area does not change if B_i contains the entire mixed cell. In this case, we have $\sum H_{ij}u_{ij} = 0$ by Minkowski's theorem for convex polygons. To compute the rate of change while aging, we note that the area of the sector spanned by $\mu_i \cap S_i$ is the area of the entire disk times the fraction of the bounding circle inside μ_i, which is $\sqrt{g_i}\, P_i/2$. With respect to age, the derivative of that sector is the same as that of $\mu_i \cap B_i$, which is therefore

$$\frac{\mathrm{d}A_i}{\mathrm{d}g_i} = \frac{P_i}{4\sqrt{g_i}}. \tag{27}$$

Case $p = 1$. We consider the body within a mixed cell μ_{ij}, as illustrated in Fig. 6. The boundary of $\mu_{ij} \cap B_{ij}$ consists of hyperbola arcs and straight line segments. When we slide the focus of the hyperbola along a vector t_{ij}, then the area within μ_{ij} changes at a rate that depends again on the lengths of the line segments and the angles they form with t_{ij}. Specifically, that rate is $(\mathrm{d}A_{ij}/\mathrm{d}z_{ij}) \cdot t_{ij}$, with

$$\frac{\mathrm{d}A_{ij}}{\mathrm{d}z_{ij}} = (H_{ji} - H_{ij}) \cdot u_{ij}^{\mathrm{T}} + (W_{ji} - W_{ij}) \cdot v_{ij}^{\mathrm{T}}. \tag{28}$$

Note that Eq. (28) can be decomposed into the terms contributed by each side of the rectangle. We use this to compute the derivative in the somewhat more complicated case of aging the hyperbola. We first observe that aging and scaling affect the hyperbola in the same way, that is, $x_1^2 - x_2^2 + (g_{ij} + \varepsilon) = 0$ defines the same hyperbola as does $c^2 x_1^2 - c^2 x_2^2 + g_{ij} = 0$ if $c = \sqrt{g_{ij}/(g_{ij} + \varepsilon)}$. The only difference between the two transformations is that aging does not affect the mixed cell while scaling does. The new area is thus $1/c^2$ times the old area minus what we lose by moving the sides of the mixed cell back to the original positions. Ignoring higher-order terms, that loss is $(\frac{1}{c} - 1)Y_{ij}$, where $Y_{ij} = H_{ij}w_{ij} + H_{ji}w_{ji} + W_{ij}h_{ij} + W_{ji}h_{ji}$. We have $\frac{1}{c^2} = 1 + \varepsilon/g_{ij}$ and, again ignoring higher-order terms, $\frac{1}{c} - 1 = \varepsilon/2g_{ij}$. To a first order of approximation, the area difference is therefore $\frac{\varepsilon}{g_{ij}}A_{ij} - \frac{\varepsilon}{2g_{ij}}Y_{ij}$. We get the derivative by dividing by ε:

$$\frac{\mathrm{d}A_{ij}}{\mathrm{d}g_{ij}} = \frac{A_{ij} - Y_{ij}/2}{g_{ij}}. \tag{29}$$

We note that for g_{ij}, the hyperbola degenerates to a pair of lines. In this case, A_{ij} is the area of the double-cone clipped to within the mixed cell. The four rectangles, whose signed areas add up to Y_{ij} cover twice as much area, which implies $A_{ij} - Y_{ij}/2 = 0$.

Case $p = 2$. The derivatives for triple-index mixed cells μ_{ijk} are similar to the ones for single-index mixed cells. Assuming the sequence ijk enumerates the vertices in a clockwise order, W_{ij}, W_{jk} and

W_{ki} are the lengths of the three edges clipped to within B_{ijk}. By translating Eqs. (26) and (27) to the triple-index case, we get

$$\frac{dA_{ijk}}{dz_{ijk}} = \sum_{ab} \left(W_{ab} \cdot v_{ab}^{T} \right), \tag{30}$$

$$\frac{dA_{ijk}}{dg_{ijk}} = \frac{P_{ijk}}{4\sqrt{g_{ijk}}}, \tag{31}$$

where the first sum ranges over all $ab \in \{ij, jk, ki\}$.

Elementary derivatives for perimeter.   All perimeter derivatives depend on the angles at which the skin meets the edges of the mixed complex. We see in Fig. 9 that the circle bounding the disk D_i meets the Voronoi edge v_{ij} at an angle $\varphi_{ij} = \arccos(2w_{ij}/r_i)$. After shrinking v_i by a factor $1/2$ to μ_i and the circle by a factor $1/\sqrt{2}$ to S_i, the angle becomes $\delta_{ij} = \arccos(\sqrt{2}w_{ij}/r_i)$. Symmetrically, we let θ_{ij} be the angle at which the circle S_{ijk} meets the shrunken Delaunay edge σ_{ij} that is an edge of the mixed cell μ_{ijk}. Since the skin is tangent continuous, the hyperbola S_{ij} meets the same edges at supplementary angles $\pi - \delta_{ij}$ and $\pi - \theta_{ij}$, on the respective other sides. All angles are measured outside the body. We compute the derivatives by considering the three types of mixed cells in turn.

Case $p = 0$. Locally within μ_i, the skin is the same as the circle S_i, which intersects each edge of μ_i in zero, one or two points. When we slide the center along the vector t_i, the perimeter changes at a rate that depends on the angles at which S_i meets the boundary, and on the angles the boundary edges form with t_i. Specifically, that rate is $(dP_i/dz_i) \cdot t_i$, with

$$\frac{dP_i}{dz_i} = \sum_{j} \left(\frac{E_{ij}}{\sin \delta_{ij}} \cdot u_{ij}^{T} \right). \tag{32}$$

Similarly, the rate of aging depends on the angles at which S_i meets the boundary of μ_i, but it also depends on the perimeter within μ_i, which is P_i. The contribution of each intersection point is minus one over the sine of the angle times the derivative of the radius. Since $r_i = \sqrt{2g_i}$, that derivative is $dr_i/dg_i = 1/\sqrt{2g_i}$. This implies

$$\frac{dP_i}{dg_i} = \frac{P_i}{2g_i} - \sum_{j} \frac{E_{ij}}{\sqrt{2g_i} \sin \delta_{ij}}. \tag{33}$$

Case $p = 1$. The hyperbola S_{ij} intersects the left, right, lower and upper sides of the mixed cell μ_{ij} in E_{ij}, E_{ji}, F_{ij} and F_{ji} points. The corresponding angles are $\pi - \delta_{ij}$, $\pi - \delta_{ji}$, $\pi - \theta_{ij}$ and $\pi - \theta_{ji}$. When we slide the focus of the hyperbola along a vector t_{ij}, the perimeter within μ_{ij} changes at a rate that depends on these angles and on the angles the sides form with t_{ij}. Specifically, the rate is $(dP_{ij}/dz_{ij}) \cdot t_{ij}$, with

$$\frac{dP_{ij}}{dz_{ij}} = \left(\frac{E_{ji}}{\sin \delta_{ji}} - \frac{E_{ij}}{\sin \delta_{ij}} \right) \cdot u_{ij}^{T} + \left(\frac{F_{ji}}{\sin \theta_{ji}} - \frac{F_{ij}}{\sin \theta_{ij}} \right) \cdot v_{ij}^{T}. \tag{34}$$

To compute the derivative of the perimeter with respect to aging, we use again the idea of simulating aging by scaling and shrinking. To increase the age to $g_{ij} + \varepsilon$, we scale the hyperbola by a factor $\frac{1}{c} = \sqrt{1 + \varepsilon/g_{ij}}$. This increases the perimeter to $\frac{1}{c}P_{ij}$. To correct for the scaling of the mixed cell, we

move the four sides back to their original positions. In doing this, we lose some of the perimeter. To first order, that loss is $(\frac{1}{c} - 1)Z_{ij}$, with

$$Z_{ij} = \frac{E_{ij} w_{ij}}{\sin \delta_{ij}} + \frac{E_{ji} w_{ji}}{\sin \delta_{ji}} + \frac{F_{ij} h_{ij}}{\sin \theta_{ij}} + \frac{F_{ji} h_{ji}}{\sin \theta_{ji}}.$$

To first order, $1/c$ is equal to $1 + \varepsilon/2g_{ij}$. The difference between the perimeter before and after the transformation is therefore approximately $\frac{\varepsilon}{2g_{ij}}(P_{ij} - Z_{ij})$. We get the derivative by dividing by ε, which gives

$$\frac{\mathrm{d}P_{ij}}{\mathrm{d}g_{ij}} = \frac{P_{ij} - Z_{ij}}{2g_{ij}}. \tag{35}$$

We note that for $g_{ij} = 0$, all angles are $\pi/2$ or $3\pi/2$. Therefore, Z_{ij} is the perimeter of the double-cone clipped to within the mixed cell, which implies $P_{ij} - Z_{ij} = 0$.

 Case $p = 2$. The derivatives for triple-index mixed cells μ_{ijk} are similar to the ones for the single-index mixed cells. Assuming again that ijk enumerates the vertices of the triangle in a clockwise order, F_{ij}, F_{jk}, and F_{ki} are the numbers of points at which the skin meets the three edges. By translating Eqs. (32) and (33) to the triple-index case, we get

$$\frac{\mathrm{d}P_{ijk}}{\mathrm{d}z_{ijk}} = \sum_{ab} \left(\frac{F_{ab}}{\sin \theta_{ab}} \cdot v_{ab}^{\mathrm{T}} \right), \tag{36}$$

$$\frac{\mathrm{d}P_{ijk}}{\mathrm{d}g_{ijk}} = \frac{P_{ijk}}{2g_{ijk}} - \sum_{ab} \frac{F_{ab}}{\sqrt{2g_{ijk}} \sin \theta_{ab}}, \tag{37}$$

where both sums range over all $ab \in \{ij, jk, ki\}$.

Continuity. We study the continuity by inspecting Eqs. (14)–(37), which flesh out the Derivative Theorem. Both the area and the perimeter derivatives are continuous almost everywhere and have measure-zero subsets of $\mathbb{R}^{3n}$ at which they are discontinuous. These subsets are smaller than the ones for the area and perimeter derivatives of a union of disks, which are studied in [6]. Furthermore, the discontinuities are milder for the body than they are for the union. This is not surprising since the difference between the two are the blending regions, which are added to the body to soften the transitions caused by the motion or growth of the input disks. There are potential discontinuities only when two disk centers approach each other, when the skin meets an edge of the mixed complex tangentially, and when the age of a circle or hyperbola vanishes. We discuss the three cases in turn.

Case $\zeta_{ij} \to 0$. Of the twelve equations, Eqs. (14)–(25), eight have the distance between two centers in the denominator. Some of these occurrences are harmless because the numerators are constant zero or because the body has an empty intersection with the corresponding mixed cells. Some occurrences, however, seem to remain and may cause the derivatives to blow up. Even if they do not blow up, the unit vectors u_{ij} and v_{ij} exhibit locally discontinuous behavior and may lead to different limits if the points of discontinuity are approached from different directions.

Case $\sin\delta_{ij}, \sin\theta_{ij} \to 0$. The six equations (32)–(37) have the sine of the angle formed by a Delaunay and a Voronoi edge in the denominator. Although the corresponding quotients blow up when this angle goes to zero or to π, the quotients cancel each other and do not cause any discontinuities in the perimeter derivative. To see this, we note that $\sin\delta_{ij}$ or $\sin\theta_{ij}$ vanish only if S_i or S_{ijk} touches an edge of the mixed complex tangentially. When the circle grows further, the arc on the other side of that edge gets replaced by a piece of a hyperbola. That piece corresponds to a blowing up quotient in the derivative of P_{ij} that cancels the one in the derivative of P_i or P_{ijk}.

Case $g_* \to 0$. Each of the six equations (27), (29), (31), (33), (35) and (37) either has $\sqrt{g_*}$ or g_* in the denominator. The numerators vanish at the same time, leading to undefined quotients $\frac{0}{0}$. Some of these quotients have finite limits, but some blow up. The quotients in Eqs. (33) and (37) blow up the fastest, but even their speed is only proportional to one over $\sqrt{g_*}$. If we differentiate with respect to the radius rather than the age, we get another factor $\mathrm{d}r_i^2/\mathrm{d}r_i = 2r_i$, which off-sets the explosive growth in all six cases. It follows that doing so eliminates the age as a source of discontinuities.

In summary, the subset of $\mathbb{R}^{3n}$ where the area and perimeter derivatives are discontinuous has dimension $3n - 1$, but if we differentiate with respect to radii instead of square radii, the dimension of that subset is at most $3n - 3$.

5. Discussion

This paper presents analytic formulas for the area, the perimeter, the area derivative, and the perimeter derivative of the body defined by a finite collection of disks in the plane. Given the filtrations of the Delaunay triangulation and of the Voronoi diagram, these formulas can be evaluated in time proportional to the number of disks. However, the formulas are fairly involved, and it would be worthwhile to double-check them, possibly experimentally by comparing the derivatives with changes computed by evaluating the area and perimeter formulas.

Although this paper completely settles the question it studies, there is much further work still to be done. The generalization of the formulas from two to three dimensions is perhaps the most important next step. It would also be interesting to analyze the second derivatives, which could be useful in accelerating the global design cycle of topology optimization. Finally, we note that three-dimensional bodies are natural representations of molecular conformations. It would thus be interesting to see whether or not the formulas developed in this paper are useful in the simulation of dynamic molecular processes. In this context, we mention the weighted area derivative of a union of balls, which is used to estimate the hydrophobic effect in implicit representations of the solvent [4]. That derivative has discontinuities along a measure-zero subset of the state space. We expect that the derivative of the area of a skin surface has fewer and milder discontinuities, which is an advantage in large scale simulations.

Appendix A

Table A.1 provides a list of notation used in this paper.

Table A.1
Notation for geometric concepts, functions, variables

$\mathcal{D}, F = \bigcup \mathcal{D}$	collection, union of disks	$\alpha, D_{i,\alpha}, \mathcal{D}_\alpha$	growth parameter, disk, collection
$\mathcal{U}, G = \bigcup \mathcal{U}$	collection, union of disks	$\beta, U_{i,\beta}, \mathcal{U}_\beta$	growth parameter, disk, collection
$D_i = (z_i, r_i)$	disk with center and radius	$F_\alpha = \bigcup \mathcal{D}_\alpha$	union of grown disks
$U_\iota = (y_\iota, s_\iota)$	orthogonal disk	$G_\beta = \bigcup \mathcal{U}_\beta$	union of grown disks
C_i, C_ι	circle bounding D_i, U_ι	K_α, V_β	α-complex, β-complex
π_i, π_ι	power distance from D_i, U_ι	A_i, A_{ij}, A_{ijk}	area within mixed cell
$\nu_i, \nu_{ij}, \nu_{ijk}$	Voronoi polygon, edge, vertex	P_i, P_{ij}, P_{ijk}	perimeter within mixed cell
$\sigma_i, \sigma_{ij}, \sigma_{ijk}$	Delaunay vertex, edge, triangle	L_{ij}, W_{ij}, H_{ij}	clipped total length, width, height
$\mu_i, \mu_{ij}, \mu_{ijk}$	mixed cell	N_{ij}, E_{ij}, F_{ij}	number of intersections with skin
h_{ij}, h_{ji}	heights of quadrant	δ_{ij}, θ_{ij}	angles at the intersection points
w_{ij}, w_{ji}	widths of quadrant	ψ_{ijk}	angle from σ_{ij} to ν_{jk}
u_{ij}, v_{ij}	orthonormal coordinate frame	$\mathbf{z}, \mathbf{t} \in \mathbb{R}^{3n}$	state, state velocity vector
ζ_{ij}, η_{ij}	coordinates in the $u_{ij} v_{ij}$-frame	$\mathbf{x}, \mathbf{a}, \mathbf{p} \in \mathbb{R}^{3n}$	gradient of X, A, P
S_i, S_{ij}, S_{ijk}	circle, hyperbola, circle	$A : \mathbb{R}^{3n} \to \mathbb{R}$	area function
B_i, B_{ij}, B_{ijk}	region bounded by S_i, S_{ij}, S_{ijk}	$P : \mathbb{R}^{3n} \to \mathbb{R}$	perimeter function
z_i, z_{ij}, z_{ijk}	focus of S_i, S_{ij}, S_{ijk}	$DA_{\mathbf{z}}$	area derivative at state $\mathbf{z}$
g_i, g_{ij}, g_{ijk}	age of S_i, S_{ij}, S_{ijk}	$DP_{\mathbf{z}}$	perimeter derivative at state $\mathbf{z}$

References

[1] M.P. Bendsøe, Optimization of Structural Topology, Shape, and Material, Springer-Verlag, Berlin, 1995.

[2] M.P. Bendsøe, C.A. Mota Soares (Eds.), Topology Design of Structures, Kluwer, Dordrecht, 1993.

[3] F. Bowman, Introduction to Elliptic Functions with Applications, Dover, New York, 1961.

[4] R. Bryant, H. Edelsbrunner, P. Koehl, M. Levitt, The area derivative of a space-filling diagram, Manuscript, 2001.

[5] H.-L. Cheng, T.K. Dey, H. Edelsbrunner, J. Sullivan, Dynamic skin triangulation, Discrete Comput. Geom. 25 (2001) 525–568.

[6] H.-L. Cheng, H. Edelsbrunner, Area and perimeter derivatives of a union of disks, Manuscript, 2001.

[7] H.-L. Cheng, H. Edelsbrunner, P. Fu, Shape space from deformation, Computational Geometry 19 (2001) 191–204.

[8] S.-W. Cheng, H. Edelsbrunner, P. Fu, P. Lam, Design and analysis of planar shape deformation, Computational Geometry 19 (2001) 205–218.

[9] H. Edelsbrunner, The union of balls and its dual shape, Discrete Comput. Geom. 13 (1995) 415–440.

[10] H. Edelsbrunner, Deformable smooth surface design, Discrete Comput. Geom. 21 (1999) 87–115.